HHS Public Access

Author manuscript

Supercond Sci Technol. Author manuscript; available in PMC 2018 March 20.

Published in final edited form as:

Supercond Sci Technol. 2017 ; 30: . doi:10.1088/1361-6668/aa5fed.

Towards Liquid-Helium-Free, Persistent-Mode MgB_2 MRI Magnets: FBML Experience

Yukikazu Iwasa

Francis Bitter Magnet Laboratory, Plasma Science and Fusion Center, Massachusetts Institute of Technology, 170 Albany Street, Cambridge MA 02139

Abstract

In this article I present our experience at the Magnet Technology Division of the MIT Francis Bitter Magnet Laboratory on liquid-helium (LHe)-free, persistent-mode MgB_2 MRI magnets. Before reporting on our MgB_2 magnets, I first summarize the basic work that we began in the late 1990s to develop LHe-free, high-temperature superconductor (HTS) magnets cooled in solid cryogen—I begin by discussing the enabling feature, particularly of solid nitrogen (SN2), for *adiabatic* HTS magnets. The next topic is our first LHe-free, SN2-HTS magnet, for which we chose Bi2223 because in the late 1990s Bi2223 was the only HTS available to build an HTS magnet. I then move on to two MgB_2 magnets, I and II, developed after discovery of MgB_2 in 2000. The SN2-MgB_2 Magnet II—0.5-T/240-mm, SN2-cooled, and operated in persistent mode—was completed in January 2016. The final major topic in this article is a tabletop LHe-free, persistent-mode 1.5-T/70-mm SN2-MgB_2 "finger" MRI magnet for osteoporosis screening—we expect to begin this project in 2017. Before concluding this article, I present my current view on challenges and prospects for MgB_2 MRI magnets.

I. INTRODUCTION

In this article I review and update work on MgB_2 magnets that we began in the mid 2000s at the Magnet Technology Division of the FBML. Actually, we started working on high-temperature superconductor (HTS) magnet technology in the mid 1990s. One area of focus was on cryogenics that would be suitable for HTS magnets operating *adiabatically* and *liquid-helium (LHe) free*, all the way up to 77 K [1]. After examining design and operation issues for HTS magnets, we concluded that addition of solid cryogen with its large thermal mass to the metal-only cold magnet chamber would benefit an LHe-free HTS magnet [2]. Note that because the HTS magnet operating temperature range matches that of solid cryogens, particularly solid nitrogen (SN2), SN2 is a natural fit to the HTS magnet.

I begin with a general introduction to superconducting MRI magnets, followed by a brief discussion on HTS magnet stability. Next, I discuss the LHe-free HTS magnet cooled in solid cryogen, promoting the enabling feature vis-à-vis thermal mass of solid cryogen, suitability of SN2 in particular to HTS magnets. Then, I describe and discuss our earliest LHe-free, SN2-Bi2223 magnet, the very first SN2-HTS magnet system that clearly demonstrated the enabling feature of SN2 for an LHe-free HTS magnet. Finally, I move on to our three MgB_2 MRI magnets, one completed in January 2016 and another to begin in

2017. Before concluding this article, I present my current view on challenges and prospects for MgB_2 MRI magnets.

1.1 Superconducting MRI Magnets

To date MRI (and NMR) magnets have been the most successful commercial applications of superconductivity. Proliferation of these magnets began in earnest starting in the 1980s. By this time, solution to each of the design and operation issues specific and common to these magnets has emerged to enable them to be profit-making commercial products. These issues include: 1) superconductor itself, particularly technology of NbTi, the staple of both magnets, then, now, and most likely through at least the next decade; 2) techniques to make superconducting joints; 3) adiabatic stability; and 4) self-protecting techniques.

Since the early 1980s when Oxford Instruments first began marketing whole-body superconducting MRI magnets, NbTi has remained every MRI magnet manufacturer's superconductor of choice. At the outset the design approach adopted by Oxford Instruments and other manufacturers to make the magnet economically viable was *adiabatic*, i.e., *no local cooling* by liquid helium within the winding. Not locally cooled, these adiabatic NbTi magnets with not much "energy margins" [3] suffered, especially in the early years, from premature quenches, triggered primarily by mechanical disturbances [3]. Although these "high-performance" NbTi magnets, not only for MRI but also for other applications, no longer are afflicted by mechanical disturbances as relentlessly as once were, they still are, some of the times. Enter HTS and a new era for superconducting magnet technology began that impacted key design concepts, including stability [1]. Table 1 lists selected values of T_{op}, $\Delta T_{op} \equiv T_{cs} - T_{op}$, where T_{op} is the operating temperature and T_{cs} is the current-field-dependent current-sharing temperature at which critical current $I_c > I_{op}$ at T_{op} drops to $I_c = I_{op}$. Δe_h is the enthalpy density stored in the conductor between T_{cs} and T_{op}, i.e., the energy density margin. As may be inferred from Δe_h in Table 1, in adiabatic magnets of REBCO and MgB_2, stability is a non-issue against mechanical disturbances.

1.2 LHe-Free SN2-HTS Magnet

The design concept to combine a liquid-helium (LHe)-free high-temperature superconducting HTS magnet and solid cryogen, particularly solid nitrogen (SN2), was first proposed in 1997 as a superconducting "permanent" magnet [2]. Thermally and mechanically decoupled from its cooling source (i.e., a cryocooler) and operating in persistent mode, a superconducting "permanent" magnet would easily provide a field well above that possible with a conventional permanent magnet, i.e., > 0.5 T, and also over an extended period of time, this period determined by the thermal mass provided by solid cryogen and heat input to the cold chamber. The LHe-free superconducting permanent magnet has two key components: 1) persistent-mode HTS magnet; and 2) a volume of SN2 enough to keep the persistent-mode field over a period of time deemed "permanent."

1.3 Thermal Mass

One prominent role of the LHe-cooled magnet often overlooked is the thermal mass of LHe itself, i.e., a volumetric latent heat of vaporization of 2.6 MJ/m^3 at 4.2 K. By comparison, the volumetric enthalpy of copper, e.g., from 4.2 K to 4.5 K, of ~0.3 kJ/m^3, is only

~1/10,000th that of LHe: LHe is a large thermal mass reservoir and anchors the magnet at 4.2 K against heat input from outside and dissipation within the magnet winding.

1.4 Solid Nitrogen (SN2)

In the absence of LHe, the LHe-free magnet, comprising materials all of low heat capacities, has practically no thermal mass. For reliable operation the thermal mass of an LHe-free superconducting magnet should be significantly enhanced. Solid cryogens are excellent for this purpose [2, 3]. Figure 1 presents heat capacity, C_p, vs. T plots of solid cryogens—neon (SNe) and nitrogen (SN2)—and metals, lead (Pb), silver (Ag), and copper (Cu) [3]. Pb is used often as a heat capacity enhancer in cryogenic equipment, Cu is the most widely used matrix metal in LTS, and Ag is the matrix metal of Bi2223. Because it remains solid up to 63.2 K, is inexpensive (~1/50th the cost of LHe, and more significantly, with stable price), lighter (~1/10th the density of lead), electrically insulating, and nontoxic, SN2 is an excellent thermal mass enhancer for the LHe-free magnet. For example, a BSCCO or YBCO magnet may operate over the temperature range ~10–60 K, and an MgB_2 magnet 10–30 K. In the range 4.2–4.5 K, SN2 has an enthalpy density of 15 kJ/m^3, ~50 times that of copper but ~1/200th that of LHe. Thus, SN2 rather than epoxy would be a much superior impregnating material for stability of an adiabatic NbTi magnet.

Figure 2 shows $T(t)$ plots of 1-liter volumes of SNe, SN2, Pb, and Cu, under a heat input of 1 W in the range 4.2 K–60 K (4.2 K–25 K for SNe); it also has a dotted horizontal line at 4.2 K for 1 liter of boiling 4.2-K LHe [3]. The figure indicates that among these substances, SNe and SN2, also weighing ~1/10th Pb and Cu, are great thermal mass enhancers in the ranges, respectively, 4–25 K and 10–60 K. Because SNe is at least one order of magnitude more expensive than SN2, unless an extra thermal mass of SNe is needed, we may conclude that SN2 is the best thermal mass enhancer for most LHe-free magnets.

2. 1st SN2-HTS Magnet

2.1 Bi2223 Magnet

The very first proof-of-concept SN2-HTS magnet was completed in 2001 [4, 5]. The HTS magnet is an assembly of 6 series-connected double-pancake (DP) coils, each wound with Bi2223 tape. Table 2 lists magnet and Bi2223 tape parameters. Figure 3 shows a schematic drawing of the apparatus.

In this very first experiment in which the principal goal was to validate the benefit of an SN2 thermal mass, *LHe* was the cooling source to solidify the liquid nitrogen (LN2). Figure 4 depicts the method by which LHe was used to cool the system from 77 to 20 K.

The magnet and a persistent-current switch (PCS) are housed inside of a copper container (referred to as the cold body) that is suspended inside of an aluminum cryostat. The vertical walls of the cold body consist of two copper tubes, one inside the other to form an annulus. The inner tube is necessary to permit the room-temperature (RT) bore to extend down into the field of the magnet. Three access tubes lead from the RT flange at the top of the cryostat to the cold body. One tube provides a path for filling the container with LN2 and the exit of nitrogen gas (N2) during warm-up, while the other two provide a path for circulating LHe

through the helium coil in order to cool the cold body and its contents to ~15 K. These tubes also function as the structural supports for hanging the cold body within the cryostat from the RT flange. We could have reduced heat leak through the access tubes by using bends and elbows to increase the length. However, this would complicate construction of the system because an additional structure for supporting the cold mass would be required, while only a moderate reduction in heat leak would be achieved because other sources make larger contributions to the overall heat leak.

The cold body was first filled with ~1.6-liter of LN2. For cooling down, the helium flow from the LHe dewar was adjusted to maintain the cold body wall close to 65 K (above 63.2 K, the N2 freezing point) and replenishing the N2 from an N2 cylinder. This procedure permitted the N2 to condense into a liquid, creating a denser solid than a solid condensed directly from a gas. Additionally, condensing the gas as a liquid prevented overfilling the container with subcooled solid, which could have led to damaging stresses when the cold body warmed and the SN2 expanded. When the cold body was full of liquid, the N2 gas flow rate dropped, at which time the N2 input tube was sealed with a stopper. The helium flow was increased to cool the cold body to 15 K. After the experiments were completed, the system was permitted to warm above 65 K and the pressure within the cold body rose to atmospheric, the amount of N2 in the cold body was measured by a volumetric flow meter, after the cold N2 vapor was warmed to room temperature.

2.2 Magnet Performance

Although equipped with a PCS, because of 7 resistive joints in this 6-DP coil magnet, it was impossible for the magnet to operate in persistent mode during 1.2 days that warmed the cold body from 20 K to 40 K. The measured initial (at 20 K) decay time constant was ~4 hours. With a self inductance of 50.4 mH (Table 2), this gives an effective circuit resistance of ~4 $\mu\Omega$. The observed field decay rate, however, became greater as the cold body warmed. This is because the magnet critical current, I_c, decreased with temperature, accelerating field decay. Thus, to keep a field persistent over a temperature span, not only the joints must be superconducting but also the operating current must be less than I_c at the warmest end of the temperature range.

Warming Trend—With the pump-out port valve closed the cryostat pressure rose from 2 μ torr at 20 K to 20 μ torr at 40 K. The measured magnet-SN2 cold chamber temperature vs. time trace looked exactly like the SN2 trace shown in Fig. 2, except it took 1.2 days to reach 40 K with an effective average heat input of 550 mW. Also as with the SN2 plot in Fig. 2, the cold chamber temperature remained at 35.6 K for a period of time, here, ~0.5 day, owing to the latent heat (8.3 J/cm^3) of the SN2 phase.

This SN2 thermal mass enhancer design concept for the LHe-free magnets has been studied by others [6–19]. It should be noted here that GE was the first manufacturer in the early 1990s to market LHe-free superconducting MRI magnets when it introduced all-Nb_3Sn, cryocooled MRI magnets operating at 10 K, the practical upper temperature for Nb_3Sn [20]. The magnets, however, had no SN2 thermal mass enhancer.

3. 2nd SN2-HTS System: MgB_2 Magnet I

In 2003 we were awarded a 3-year project by the National Institute of Biomedical Imaging and Bioengineering (NIBIB) of the National Institutes of Health in response [21] to a NIBIB Request for Application (RFA) to "develop *low-cost* MRI magnets suitable to small hospitals in *rural* communities and *underdeveloped* nations." To us *rural* and *underdeveloped* areas meant, even in 2003, an LHe-free superconducting MRI magnet. In a way, this RFA for superconducting MRI magnets for *rural* and *underdeveloped* areas recognized a new helium-scarcity era that began at about this time, confronting even urban hospitals in the developed nations.

3.1 Magnesium Diboride

For LHe-free MRI magnet, one viable superconductor option would be an HTS, simply because the cooling source for such a magnet can *more* easily be operated with a cryocooler than the NbTi magnet that must be operated close to 4.2 K with a stability temperature margin of no greater than ~1 K [3]. In 2003 we believed that magnesium diboride (MgB2), discovered in January 2001 [22], would be one HTS that in cost and performance could compete with LTS. Figure 5 presents field vs. temperature plots of MgB_2 and two LTS staples for MRI magnets, NbTi and Nb_3Sn [23]. The figure also includes three cryogens with their boiling temperatures that are suitable for these conductors.

3.2 Magnet & Performance

Because wire length available then was only up to ~1 km, Mg_2B Magnet I was composed of 10 coils, each requiring ~1-km long wire [24]; Table 3 lists its key parameters. The MgB_2 wire of 18 filaments and insulated with S-glass sleeve was manufactured by Hyper Tech Research. With twelve reels of ~1-km long *unreacted* MgB_2 wire, we wound ten coils and reacted each coil separately at 700° for 20–40 min.

The 10 coils were stacked together and fixed with tie rods. The connections between wires were soldered with 50–50 Sn-Pb solder: the joints are not superconducting at the working temperature between 10 and 15 K. The typical joint resistance is below 1 $\mu\Omega$. The magnet is enclosed inside an annular can and during the test the can is filled with nitrogen. The can is thermally connected to the 2nd stage of a GM cryocooler. The 1st stage is anchored to the radiation shield between the room temperature and the cold body.

The S-glass insulated MgB_2 prevented the wire from sticking together during the reaction. After the heat treatment, the insulation became very fragile and in some part of the wire, broken, which caused short circuits from time to time during the winding process on a metal coil former. Because of the fragile S-glass, the wire, wound with a tension of 5 N, was not packed very tightly against each other. For react-and-wind magnet fabrication, insulation such as Formvar is definitely preferable to S-glass, because it enables the winding to be tightly packed for mechanical integrity. The winding was not impregnated with epoxy. Figure 6 shows a photo of the magnet with its SN2 can removed.

Unlike liquid helium which provides cooling through evaporation, the SN2 vapor pressure in the range 10–15 K is below 10^{-13} torr. Here, the magnet operating temperature is maintained

by a cryocooler, which has a cooling power of 6 W at 10 K and 15 W at 15 K. The magnet remained in the low temperature range even when the cryocooler was temporarily shut down, e.g., power outage, for a short period of time. Also, sometimes it is necessary to turn off the cryocooler intentionally to eliminate its vibration to create a noise-free measurement environment. For these applications, as discussed earlier a volume of SN2 in the cold body acts as a thermal mass enhancer. The SN2 used in our system was 50 liters.

Thermal conduction is crucial to maintain a uniform temperature within the winding. Table 4 lists the thermal conductivities, *k*, of LHe, SN2, and epoxy (Stycast 2850 FT) at 5 K, 10 K, and 15 K [3]. Note that at ~10 K and below, SN2 is at least an order of magnitude better thermal conductor than epoxy. If conduction cooling is critical in this temperature range, it seems better not to cast the winding inside epoxy. This point is well demonstrated by this SN2 immersed magnet: a temperature difference of only <1 K was measured between a location nearest and that farthest away from the cryocooler 2nd stage. Note that unlike most LHe-free magnets that require additional conductive thermal passages to achieve a uniform temperature in the windings, this magnet and an MgB_2 Magnet II discussed next relied only on SN2, i.e., no epoxy.

Quench and Damage—As stated earlier the S-glass insulation of the MgB_2 wire becomes very brittle and fragile after heat treatment of the wire. During the winding short circuits to the copper coil form happened from time to time. Although whenever a short was detected, the part of coil was rewound until the short was removed, we still observed signs of shorting between winding and the copper coil form during the magnet operation when field-induced stress on the wire was increased with current. Such a short circuit triggered a premature quench in this magnet at 79 A: the quench occurred in the top coil after a quiescent period of operation at 79 A for more than 30 s. We believe that the quench was caused by local heating generated at a short between the top coil and its copper coil form. Without proper protection, the top coil was damaged after this quench. Figure 7 shows a photo of the burned-out winding section of the top coil.

3.3 Superconducting Joints

Unreacted MgB_2 Wires—In 2008 we developed and published a technique to make a superconducting joint with multifilamentary *unreacted* MgB_2 [25]. The technique, however, is much more reliable with *monofilament* MgB_2 wires. The flux jumping criterion indicates that, because of its large temperature margin, MgB_2 monofilaments up to ϕ1 mm should be free of flux jumping [3]. We first verified this conclusion experimentally and demonstrated that superconducting joints could be made reliably with monofilament MgB_2 wire [26, 27]. Thereupon, we were on our way to complete a persistent-mode 0.5-T MgB2 magnet, described next. In applying our original splicing technique, we have modified it to be applicable at a sintering temperature (for 90 min.) of 700°C, a combination of temperature and duration required to react the coil winding itself. This is important because our MRI magnet will apply the wind-and-react procedure.

The process that produces higher joint critical currents with better reproducibility includes: 1) aligning the fragile filaments in the powder-pressing direction; 2) eliminating filament

breakage; 3) maximizing the joint surface area with an acute angle cut [27]. The following steps are involved: 1) etch the Cu and Monel with nitric acid; 2) shear filament at acute angle; 3) fill billet with pre-mixed Mg+B powder and insert copper plug into the billet without pressure; 4) insert the two wires into the billet in the opening between the copper flat surface and billet, aligning wires so that the angle-cut surfaces face each other; 5) insert the copper plug and press to partially seal the top of the billet; and 6) use a ceramic paste to completely seal the billet top.

We tested 10 superconducting joints of monofilament MgB2 wires at 10 K, 15 K, and 20 K in self field, measured by the 4-probe method [27], the results of which are summarized in box-and- whisker plots of Fig. 8—note that because of our test setup limit, the 10-K data are truncated at 400 K. Note also that at 15 K, 9 joints have critical currents of ≥215 A, with a maximum at 370 A, quite sufficient for joints operating at 100 A in a field < 1 T.

With Reacted MgB_2 Wires—For a magnet with a conductor that requires heat treatment, e.g., Nb_3Sn (LTS) and MgB_2 (HTS), the react-and-wind procedure is generally preferable to the wind-and-react procedure, because it eliminates the need to heat treat the magnet that necessarily includes materials besides the conductor. Also, an oven that can heat treat a "large" wind-and-react magnet will not be necessary. Nevertheless, we chose to wind-and-react our magnet because it is much easier to handle MgB_2 wire unreacted than reacted. Also, each of our 10 coils was small enough for heat treatment. Even for our magnet in which joints are made of *unreacted* wires, it is important to develop a technique to make superconducting joints with *reacted* MgB_2 wires [28, 29]. Although in our magnet we had no plan to repair defective joints after they had been *reacted*, because it is inherently useful to be able to replace defective joints, we decided to develop, as a backup plan, a technique for *reacted* wires based on our technique for unreacted wires.

The rig is quite similar to the one used to make joints with unreacted wires; to achieve higher powder compacting pressure a stainless steel plug, rather of copper, was used to compress the Mg+B power. Figure 9 shows $V(I)$ plots at 10 K of *reacted* MgB2 wire joints for three compressive pressures [30]. Even at 0.85 GPa, a joint has a critical current at 10 K in self field of only 86 A; our activity on this technique is a work in progress.

4. 3rd SN2-HTS Magnet: MgB_2 Magnet II

Although HTS magnets are much tolerant of the disturbances that still afflict LTS magnets [3], unprotected, they can be damaged, as demonstrated by our unprotected SN2-MgB_2 Magnet I—see Fig. 7. Thus, we did apply an active protection technique to our SN2-MgB_2 Magnet II. Began in 2010 and completed in January 2016, this SN2-MgB_2 Magnet II generated a persistent-mode center field of 0.496 T at 100 A [31, 32]. Because this magnet and its results are described by Ling and others in the same Special SUST Issue [33] as this article, here I will refrain from reporting on this magnet in detail.

4.1 MgB_2 Magnet II

The magnet, 460-mm long overall, was of 8 coil-PCS-joint-modules, each coil 276-mm winding ID and 290-mm OD and wound with the same Hyper Tech Research unreacted

wire. A circuit model of a coil-PCS-joint module is shown in Fig. 10a; photos of a module with its PCS and joint are shown in the foregrounds, respectively, of Figs. 10b and c; Fig. 10d shows a photo of eight modules ready for assembly, schematically drawn in Fig. 10e, which also shows a cryocooler and a cooling coil; LHe was forced through the cooling coil to accelerate the initial cooldown proccess [32].

4.2 SN2

A 60-kg (≃ 58 liters in the range 10–20 K [3]) SN2 mass in this magnet dramatically enhanced the thermal mass of the magnet-SN2 cold chamber, as illustrated in the experiment. Figure 11 shows a graph of the center field (black) and magnet temperature (red) vs. time plots when the cold body started receiving an extra amount of heat, caused by a defective vacuum seal [32]. The rising temperature curve (dotted red) gives $dT/dt = 0.8$ mK/s. The net enthalpy changes from 11.5 K to 12.5 K for the 50-kg magnet and 60-kg SN2 are, respectively, 0.25 kJ and 17 kJ [3]. This translates to a net heat input of 13 W to the magnet-SN2 chamber. If it were not for this 60-kg SN2, the magnet temperature would have risen at $dT/dt = 50$ mK/s, as indicated by the blue dashed line, demonstrating that SN2 is indeed effective in moderating dT/dt in an LHe-free magnet. Note that the center field remains constant during this rising temperature excursion.

4.3 Current Distribution Among Modules

For MgB_2 technology that is not as developed as those of NbTi and Nb_3Sn, dividing this magnet into 8 coil-PCS-joint modules has proven successful. It certainly reduced risk and led to a successful magnet, though magnet manufacturing process is time-consuming. One shortcoming that became evident was a nonuniform current distribution among 8 modules as the magnet slowly warmed up from 9 K (0.5-T center field) to 14 K over a period of a few days. Figure 12 shows a persistent-mode current in each module at 13 K corresponding to this field profile as computed with the least square method [32]. Of 8 coil-PCS-joint modules, 4 modules could not sustain a persistent current of 100 A at 13 K (0.47-T center field). For example, in the leftmost coil in Fig. 12 (bottom coil in Fig. 10e), the critical current of *at least one component* of the coil-PCS-joint module was 47.9 A. Similarly in the 3 other “low performers” the critical currents were respectively 77.5 A, 76.9 A, and 76.6 A.

If this magnet were a commercial product, the manufacturer would have two options to salvage this magnet: 1) replace the 4 low performers; 2) restrict the operating temperature range to between 9 K and a high end, say, 11 K, at which these low performers can still sustain 100 A in persistent mode. The manufacturer would very likely opt for Option 2.

4.4 Protection

One innovative idea introduced in this 8-coil-PCS-joint magnet is to make each PCS in the module not only act as a switch but also provide enough resistive-state mass to enable the coil to remain at < 200 K after it absorbs the entire coil energy. For a total energy of 3.7 kJ stored in the magnet at 100 A, a total PCS MgB_2 wire length of 156 m was deemed enough, ~20-m long in each PCS. Forced quenches at 100 A confirmed that magnet could be protected with this PCS design. The magnet persistent-mode operation, its protection performance, and other details are described in [32, 33].

4.5 Comments on Modularization

This 8-module procedure was an apt choice for two reasons in *2012:* 1) our MgB_2 magnet technology (coil; PCS; joint; protection) had not been developed well enough, in contrast to those of NbTi and Nb_3Sn, to risk a more economic one-module approach; 2) MgB_2 *conductor* technology had not reached the stage to enable the conductor manufacturer to produce *uniform-quality* (superconductivity, mechanical, metallurgical properties) wire of length >300 m, forcing at any rate a modular approach even if the MgB_2 magnet technology had then been advanced well enough for a one-module magnet. Modularization is actually a standard manufacturing approach with commercial MRI magnets of NbTi and Nb_3Sn chiefly because of stress, conductor grading, and protection issues. In light of this standard modularization already practiced, the fact that it also worked well with an MgB_2 magnet as demonstrated by our magnet is indeed encouraging. We believe that our success with this MgB_2 magnet will impact the next generation MRI magnets.

5. 4th SN2-HTS Magnet: MgB_2 Magnet III

The MgB_2 MRI Magnet III described here is for osteoporosis screening [34]. This 5-year program is expected to start in 2017.

5.1 MRI of Metabolic Bone Disease

MRI of bone mineral and bone matrix ("solid-state MRI") can separately measure both mineral (the commonly understood meaning of "bone density") [35] and matrix content [36], and therefore can distinguish osteoporosis from osteomalacia [37]. High spatial-resolution MRI can image the microarchitecture of the trabecular network as well as cortical thickness, providing full 3D statistical measures of the trabecular network that traditionally were estimated from 2D sections using histomorphometry.

5.2 LHe-Free, Persistent Mode MgB_2 "Finger" MRI Magnet

Our proposed tabletop MgB_2 "finger" MRI magnet may possibly be the first MRI magnet targeted exclusively for osteoporosis screening. With ~10 million people currently suffering from osteoporosis in the U.S. alone [38, 39], the tabletop "finger" MRI magnet may likely find a niche in the MRI magnet marketplace.

The key parameters of an MgB_2 "finger" MRI magnet based on our first-cut design are given in Table 5, with Fig. 13 showing a magnet cross section (a) and three circuit models (b)–(d) [34]. The main coils (M1 & M2: large blue blocks), each with 90-mm ID, provide a 70-mm room-temperature (RT) bore and a ϕ25-mm RT center space for a finger, leaving an annular space, 70^{-}-mm OD, and 25^{+}-mm ID for gradient and shim coils. The correction coils (C1 & C2; small blue rectangles), each with 140-mm ID, are large enough for a ϕ102-mm RT access for a folded hand. Each coil will be wound with unreacted, insulated MgB_2 ϕ1.0-mm wire. The magnet also contains an iron yoke cylinder (grey rectangles).

5.2.1 Modular Options—For this MgB_2 "finger" MRI magnet, three options are possible, as shown in Figs. 13b–d circuit models. In the 1st and 2nd options (Figs. 13b, c), the magnet is composed of two 2coils-PCS-2joints modules. In the 3rd option (Fig. 13d), all components

are in one module. We will choose either the 2nd or 3rd option. In the 2nd option, if two loops have different persistent currents, we may: 1) replace a low-performance set with a new set or 2) as demonstrated in the 8-module magnet, reduce the maximum T_{op} from 17 K to, say, 15 K, enough to make the low-performance set to carry the same current as the good-performance set. The 2nd option with two suboptions may be less risky than the 3rd option. For this magnet, destined in Year 5 to be operated for osteoporosis screening, both loops must carry the identical persistent current of 107.9 A. Also, after experience with building 10 coil-PCS-joint modules, two of which failed in our previous MgB_2 magnet, we are confident of successfully completing this MgB_2 "finger" MRI magnet.

5.2.2 Iron Yoke—The iron yoke contributes an extra field to the center, shields the magnet from an extraneous field, and limits the fringe field in the magnet vicinity. For computation its $M(H)$ was divided into three regions: linear (μ/μ_o = 1730) to M =1.4 T, linear-to-saturation transition; and saturation (M_s = 1.9 T). The magnet generates fields of 1.5 T (center) and 2.0 T (peak) at an operating current of 107.9 A. This MgB_2 wire has I_c = 145 A at 2 T and 17 K. Therefore, the magnet will be able to operate in persistent mode up to 17 K or even 20 K. Without the yoke the magnet generates 1.38 T. Also, the iron yoke limits a fringe field to < 5 gauss in immediate vicinity of the magnet. Equally important, the iron yoke shields the magnet center region from extraneous fields generated outside this magnet system.

5.2.3 SN2—In addition to the coils and the iron yoke, the cold chamber stores ~10 kg (~10 liters) of SN2. Unlike the previous system that had ~60 kg of SN2, we believe that ~10 kg is sufficient for this system: the SN2 enthalpy of 10 kJ [3] for an estimated net heat input of ~0.25 W with the cryocooler off will prolong a temperature rise from 14 to 17 K to a period of ~10 hours. Note that in contrast, the 35-kg iron yoke has a thermal mass of <1 kJ.

5.3 Overall System

Figure 14 shows schematic views of the overall system [34]: (a) side; and (b) bottom. As seen in Fig. 14a, the first part of a 2-step RT bore is a ϕ102-mm, 120-mm deep bore for a folded hand to penetrate. Of the second ϕ70-mm bore, the center ϕ25-mm is for the tip of a finger to reach the magnet center 50-mm away.

Mechanical Support—The main support components are 4 thin-walled stainless steel cylinders, 2 within the cold chamber, one for the coils and the other for the iron yoke. The cold chamber is supported by a 0.5-mm wall cylinder, which in turn is supported by another cylinder to the room-temperature flange. The system mass, including the cryocooler coldhead, is ~100 kg. The entire system is anchored to an L-shaped ring attached to the cryostat outer wall (not shown in Fig. 14a), which is placed on the outer rim of a ϕ40-cm hold in the table, the top ~15 cm above the tabletop.

Stability & Protection—HTS, including MgB2, typically has a stability margin at least 100 times greater than that of LTS [3]—see also Table 1: HTS magnets are not susceptible to quench caused by disturbances that affect LTS magnets [3]. In case of a quench, the same

technique used in MgB2 Magnet II will be deployed for protection; here one PCS will have a resistive-state mass large enough to absorb the entire magnetic energy.

Temporal Stability—Within a few days after the magnet, placed in persistent-mode operation at 1.5 T, we expect the field to keep a temporal stability of < 0.1 ppm/hr.

5.4 Program Timetable and Activities

During the first 4 years of this 5-year program, the SN2-MgB_2 magnet, including shim coils and gradient coils, will be completed. In Year 5, the "finger" magnet will be used by Dr. Ackerman of the Athinoula A. Martinos Center for Biomedical Imaging at the Massachusetts General Hospital (MGH), Boston MA, and Co-Investigator of this program. Up to 30 patients will be screened for osteoporosis.

6. SN2 Safety

When dealing with a solid like SN2 that can vaporize, there always is concern with safety. No systematic study on safety dealing with SN2 has been conducted. A damaging event most likely imagined to occur involves a volume of SN2 suddenly vaporized by, e.g., a quench, leading to a large pressure within the cold body that may damage the system.

To date we have not experienced any accidents, not even minor, with our SN2-magnets. These include not only the first three SN2-HTS magnets described here but also another SN2-NbTi magnet [40]. Obviously, following a standard practice in cryogenics, each system was provided with an adequate pressure relief, as will be with our next system.

Perhaps it would be beneficial to study the transient behavior and thermodynamics of nitrogen when SN2 is exposed to a heated substance and transits into the liquid and vapor phases. Rather than relying on a few experiences of limited operation situations like ours, an affirmative answer from such a study may settle the SN2 safety issue for good.

7. Challenges & Prospects for MgB_2 MRI Magnets

As stated at the outset, NbTi magnet technology is well established and NbTi remains the conductor of choice for superconducting MRI magnets. However, there are two vulnerable areas in the NbTi MRI magnet: 1) although much less frequently than in the 1980s, NbTi MRI magnets still suffer from premature quenches triggered by minute mechanical disturbances; and 2) they rely heavily on LHe. Obviously, these weaknesses are being addressed to maintain NbTi MRI magnets' dominance as profitable products. One vulnerable area for MgB_2 magnets, actually common to all HTS magnets, is protection [3]. Although this was addressed in our SN2-MgB_2 Magnet II and the same technique applied in our "finger" MRI magnet, more work on protection is needed.

There are two challenges that must be conquered by the MgB_2 magnet before it can break through the "NbTi" barrier:

- First, MgB_2 wire. It must become as good a magnet-grade superconductor as NbTi. It needs to meet rigorous magnet specifications as a commercially

available commodity [3]. One of the magnet specifications includes “long” length (≫ 1 km), which is still a challenge to MgB_2 wire. Another requirement equally important is the price of MgB_2 wire: it should be no greater than a few times that of an NbTi wire of the same specifications.

- Second, MgB_2 MRI magnet. It cannot be a direct replacement to the NbTi MRI magnet. It must provide enabling features that would eradicate the two vulnerabilities of the NbTi magnet. These features must be exploited in full. One obvious solution: operation of the MgB_2 MRI magnet, LHe-free, cryocooled, and at well above 4.2 K.

One way for the MgB_2 MRI magnet to penetrate into marketplace is in niche applications: our tabletop MgB_2 “finger” MRI magnet for osteoporosis screening may be a good candidate for such an application.

8. Conclusions

To date three SN2-HTS magnets have been built and operated at the Magnet Technology Division of the MIT Francis Bitter Magnet Laboratory. Each SN2-HTS magnet has demonstrated that the enabling feature of SN2, dramatically enhancing the magnet’s effective thermal mass in the temperature range suitable for LHe-free HTS magnets. Recent completion of a 240-mm bore SN2-MgB_2 MRI magnet operated in persistent mode reinforces this point. We believe that our 4th, a tabletop 1.5-T/70-mm “finger” MRI magnet for osteoporosis screening, scheduled to begin in 2017, is a viable application of MgB_2 for MRI magnets. When the *price of MgB_2 wire approaches that of NbTi wire*, MgB_2 should become a realistic superconductor option for the next generation of marketplace MRI magnets, with initial application in a niche area such as for osteoporosis screening.

Acknowledgments

I thank the Korea Electrotechnology Research Institute and Daesung Cable Co., Korea for supporting our very first SN2-HTS magnet project. Since then the National Institute of Biomedical Imaging and Bioengineering of the National Institutes of Health has been the primarily supporter of our SN2-MgB_2 magnet development activities. I am also grateful to those involved in the projects described in this article: FBML colleagues, past and present; former students; postdocs; and visiting scientists. Chronologically, they include: Benjamin Haid (now at the Lawrence Livermore National Lab); Haigun Lee (Korea University); Juan Bascuñán; Seungyong Hahn (NHMFL/FSU); Weijun Yao (ORNL); Woo-Seok Kim (Korea Polytechnic U); Dong Keun Park; Jiayin Ling (GE Healthcare); John Voccio (Wentworth Institute of Technology); Youngjae Kim (NHMFL); Jungbin Song (Korea University). I would also like to thank Timing Qu (Tsinghua U) and Minchul Ahn (Kunsan U) for their contribution to the first-cut design of the “finger” MRI magnet; Jerome Ackerman of the MGH and Co-Investigator of this “finger” magnet project for his help in preparation of the NIH applications; Seungyong Hahn, Juan Bascuñán, John Voccio, and Jiayin Ling for their critical edits of the first manuscript. I also thank the reviewers of the first manuscript for their constructive suggestions and insightful questions, most of which I have incorporated (suggestions) and responded to (questions) in the revised manuscript; I am grateful to Philip Michael for his constructive comments on an earlier revised manuscript. Finally, I’m also grateful to Benjamin Haid and Jiayin Ling for making new versions, respectively, of Figures 3 and 8.

References

1. Iwasa Y. Design and operational issues for 77-K superconducting magnets. IEEE Trans Mag. 1988; MG-24:1211.
2. Iwasa, Y. A ‘permanent’ HTS magnet system: key design & operational issues Advances in Superconductivity X. Springer-Verlag; Tokyo: 1998. p. 1377

3. Iwasa, Y. Case Studies in Superconducting Magnet. 2nd. Springer; 2009.
4. Haid, BJ. PhD Thesis. Department of Mechanical Engineering, M. I. T.; Cambridge, MA: 2001. A 'permanent' high-temperature superconducting magnet operated in thermal communication with a mass of solid nitrogen.
5. Haid B, Lee H, Iwasa Y, Oh S-S, Kwon Y-K, Ryu K-S. A "permanent" high-temperature superconducting magnet operated in thermal communication with a mass of solid nitrogen. Cryogenics. 2002; 42:229.
6. Jo Y-S, Kwon Y-K, Sohn M-H, Ryu K-S, Hong J-P, Lee J. Temperature characteristics of rotor of HTS synchronous rotating machine cooled by solid nitrogen. Physica C. 2002; 372–376(4):1535.
7. Nakamura T, Muta I, Okude K, Fujio A, Hoshino T. Solidification of nitrogen refrigerant and its effect on thermal stability of HTSC tape. Physica C. 2002; 373–376(4):1434.
8. Nakamura T, Higashikawa K, Muta I, Fujio A, Okude K, Hoshino T. Improvement of dissipative property in HTS coil impregnated with solid nitrogen. Physica C. 2003; 386(4):415.
9. Nakamura T, Higashikawa K, Muta I, Hoshino T. Performance of conduction-cooled HTS tape with the aid of solid nitrogen-liquid neon mixture. Physica C. 2004; 412–414(4):121.
10. Hales P, Jones H, Milward S, Harrison S. Investigation into the use of solid nitrogen to create a 'Thermal Battery' for cooling a portable high-temperature superconducting magnet. Cryogenics. 2004; 43(7):109.
11. Hales P, Hirst P, Milward S, Harris S, Jones H. A solid-nitrogen cooled high-temperature superconducting magnet for use in magnetohydrodynamic marine propulsion. IEEE Trans Appl Supercond. 2006; 16(4):1419.
12. Manabe T, Nakamura T, Yamada Y. Heat transfer characteristics of HTS tape impregnated with solid nitrogen-solid neon hybrid refrigerant. Physica C. 2008; 468(5):2156.
13. Song JB, Kim KL, Kim KJ, Lee JH, Kim HM, Kim WS, Yim SW, Kim H-R, Hyun OH, Lee HG. The design, fabrication and testing of a cooling system using solid nitrogen for a resistive high-T_c superconducting fault current limiter. Supercond Sci Technol. 2008; 21(8):115023.
14. Wang Q, Dai Y, Song S, Wen H, Bai Y, Yan L, Kim K. A 30 kJ Bi2223 high temperature superconducting magnet for SMES with solid-nitrogen protection. IEEE Trans Appl Supercond. 2008; 18(4):754.
15. Choi JH, Choi JW, Lee H, Song JB, Kim HJ, Seong KC, Kim SH. A study on the electrical insulation properties of solid nitrogen for cooling of the high temperature superconducting systems. Physica C. 2009; 469(4):1866.
16. Higashikawa K, Nakamura T. Cooling performance of hybrid refrigerant of solid nitrogen and small amount of neon for the purpose of HTS power applications. Physica C. 2009; 469(5):1910.
17. Song JB, Kim KJ, Kim KL, Lee JH, Kim HM, Lee GH, Chang HM, Park DK, Ko TK, Lee HG. Thermal and electrical stabilities of solid nitrogen (SN2) cooled YBCO caoted conductors for HTS magnet applications. IEEE Trans Appl Supercond. 2010; 20(4):2172.
18. Song JB, Kim KL, Yang DG, Jang JY, Ko TK, Ahn MC, Lee HG. Normal zone initiation and propagation characteristics of a solid nitrogen cooled GdBCO racetrack pancake coil. IEEE Trans Appl Supercond. 2012; 22(4):4701704.
19. Song JB, Kim KL, Yang D, Kim Y-G, Lee J, Ahn MC, Lee H. High-T_c superconducting high gradient magnetic separator using solid nitrogen cooling system for purification of CMP wastewater. IEEE Trans Appl Supercond. 2013; 23(4):3700505.
20. Laskaris ET, Ackermann R, Dorri R, Gross D, Herd K, Minas C. A cryogen-free open superconducting magnet For interventional MRI applications. IEEE Trans Appl Supercond. 1995; 5:163–168.
21. Iwasa Y. Development of a low-cost MgB2/solid N2 MRI magnet. Application to the Nationa Institutes of Health. 2003 unpublished.
22. Nagamatsu J, Nakagawa N, Muranaka T, Zenitani Y, Akimitsu J. Superconductivity at 39 K in magnesium diboride. Nature. 2001; 410(6824):6364.
23. Larbalestier DC. MgB2–A large scale applications perspective. APS March meeting MgB2 Press Brief. 2001
24. Yao W, Bascuñán J, Kim W-S, Hahn S, Lee H, Iwasa Y. A solid nitrogen cooled MgB2 'demonstration' coil for MRI applications. IEEE Trans Appl Superconduc. 2008; 18:912.

25. Yao W, Bascuñán J, Hahn S, Iwasa Y. A superconducting joint technique for MgB_2 round wires. IEEE Tran Appl Superconduc. 2009; 19:2261.
26. Ling, J. SM Thesis. Department of Mechanical Engineering, M.I.T.; Cambridge, MA: 2012. Monofilament MgB_2 wires for MRI magnets.
27. Ling J, Voccio J, Kim Y, Hahn S, Bascuñán J, Park D, Iwasa Y. Monofilament MgB_2 wire for a whole-body MRI magnet: superconducting joints and test coils. IEEE Trans Appl Superconduc. 2013; 23:6200304.
28. Patel D, Shahriar Md, Hossain A, See KW, Xu X, Barua S, Ma Z, Choi S, Tomsic M, Kim JH. MgB_2 superconducting joints for persistent current operation. Supercond SciTechnol. 2015; 28(2015)
29. Tanaka H, Kodama M, Ichiki Y, Kusunoki T, Kotaki H, Suzuki T, Nishi K, Okamoto K. Persistent current operation of conduction cooled MgB_2 coils with multifilamentary wires. Presented at the 2016 Applied Superconductivity Conference in Denver. 2016
30. Voccio P, Song J. Francis Bitter Magnet Laboratory. 2013 unpublished data.
31. Ling J, Voccio J, Hahn S, Kim Y, Song J, Bascuñán J, Iwasa Y. Development of a 0.5-T/240-mm MgB_2 MRI Magnet: Assembly Design and Module Coils. IEEE Trans Appl Supercond. 2014; 24:4400805.
32. Ling, J. PhD Thesis. Department of Mechanical Engineering, M.I.T.; Cambridge, MA: 2016. A persistent-mode MgB_2 0.5-T/240-mm solid-nitrogen-cooled magnet for MRI.
33. Ling J, Voccio JP, Hahn S, Qu T, Bascuñán J, Iwasa Y. A persistent-mode 0.5-T solid-nitrogen-cooled MgB_2 magnet for MRI. In this Special Issue. 2016
34. Iwasa Y, Ackerman JL. Tabletop liquid-helium-free, persistent-mode 1.5-T/70-mm osteoporosis MRI magnet. Application to the National Institutes of Health. 2016 unpublished.
35. Wu Y, Ackerman JL, Chesler DA, Li J, Neer RM, Wang J, Glimcher MJ. Evaluation of bone mineral density using three dimensional solid state phosphorus-31 NMR projection imaging. *Calcif.* Tissue Int. 1998; 62:512518.
36. Cao H, Ackerman JL, Hrovat MI, Graham L, Glimcher MJ, Wu Y. Quantitative bone matrix density measurement by water and fat suppressed proton projection MRI (WASPI) with polymer calibration phantoms. Magn Reson Med. 2008; 60:14331443.
37. Cao H, Nazarian A, Ackerman JL, Snyder BD, Rosenberg AE, Nazarian RM, Hrovat MI, Dai G, Mintzopo Juulos D, Wu Y. Quantitative ^{31}P NMR spectroscopy and ^{1}H MRI measurements of bone mineral and matrix density differentiate metabolic bone diseases in rat models. Bone. 2010; 46:15821590.
38. U.S. Department of Health and Human Services. Bone health and Osteoporosis: A Report of the Surgeon General. U.S. Department Of Health And Human Services; p. 2004
39. Dempster DW. Osteoporosis and the burden of osteoporosis-related fractures. Am J Manag Care. 2011; 17:s164–s169. [PubMed: 21761955]
40. Voccio J, Hahn S, Kim Y, Ling J, Song J, Bascuñán J, Iwasa Y. A 1.5-T/75-mm magic-angle-spinning NMR magnet. IEEE Trans Appl Superconduc. 2014; 24:4300704.

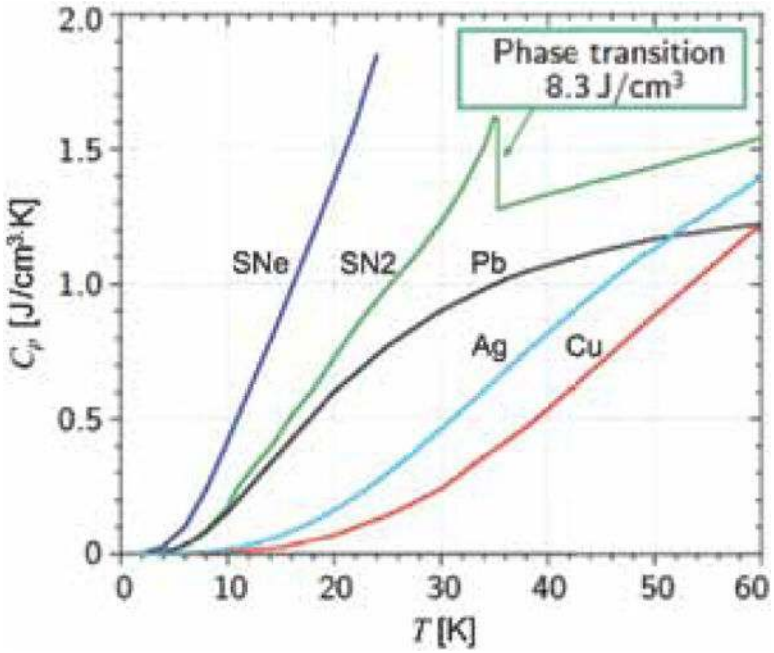

Fig. 1.

$C_p(T)$ plots of SNe, SN2, Pb, Ag, and Cu [3]. At 35.6 K SN2 absorbs an energy density of 8.3 J/cm^3 [3].

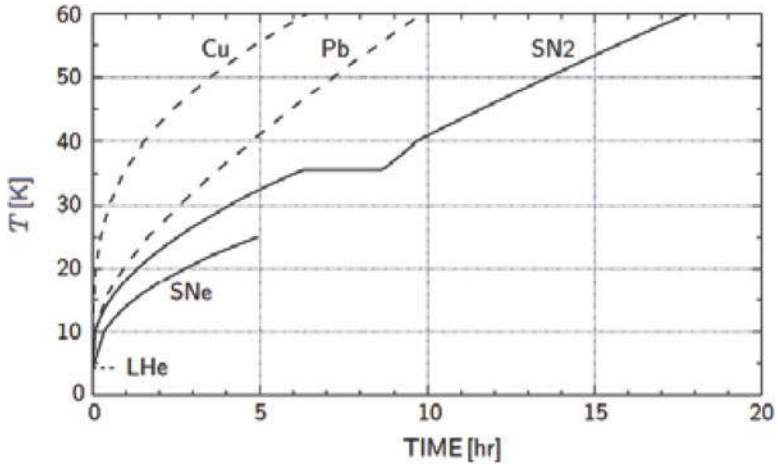

Fig. 2.

$T(t)$ plots with an initial temperature of 4.2 K for a 1-liter volume each of Cu, Pb, SN2, and SNe under a 1-W constant heat input [3]. The time required to boil off 1-liter LHe, ~0.7 hr, is shown by the dotted horizontal line at 4.2 K.

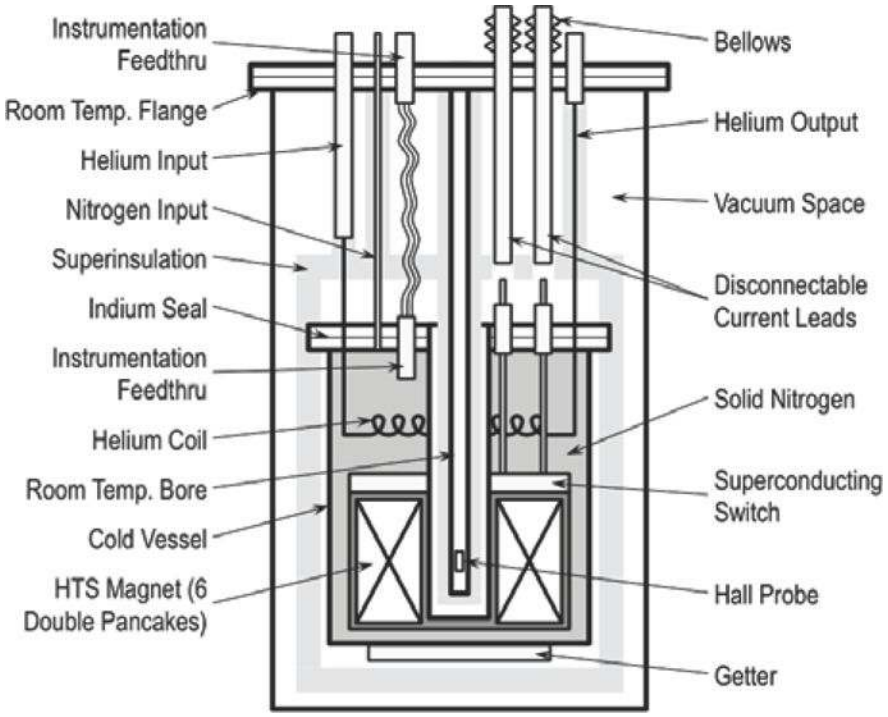

Fig. 3.

Schematic drawing of the experimental apparatus used to operate the Bi2223 magnet in thermal communication with solid nitrogen. The dimensions are in mm [4, 5].

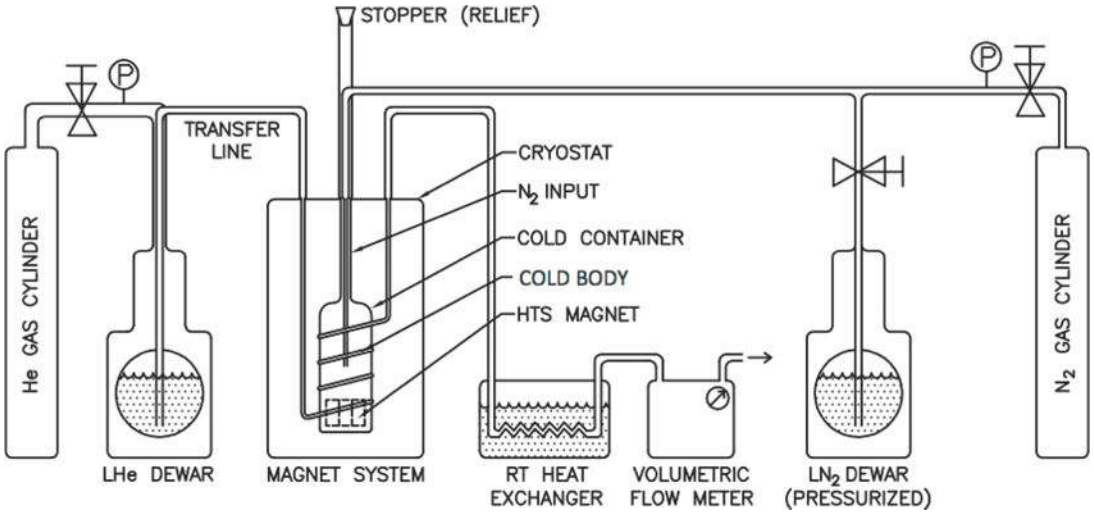

Fig. 4.
Schematics illustrating the technique for cooling the cold body to below 20 K [4, 5].

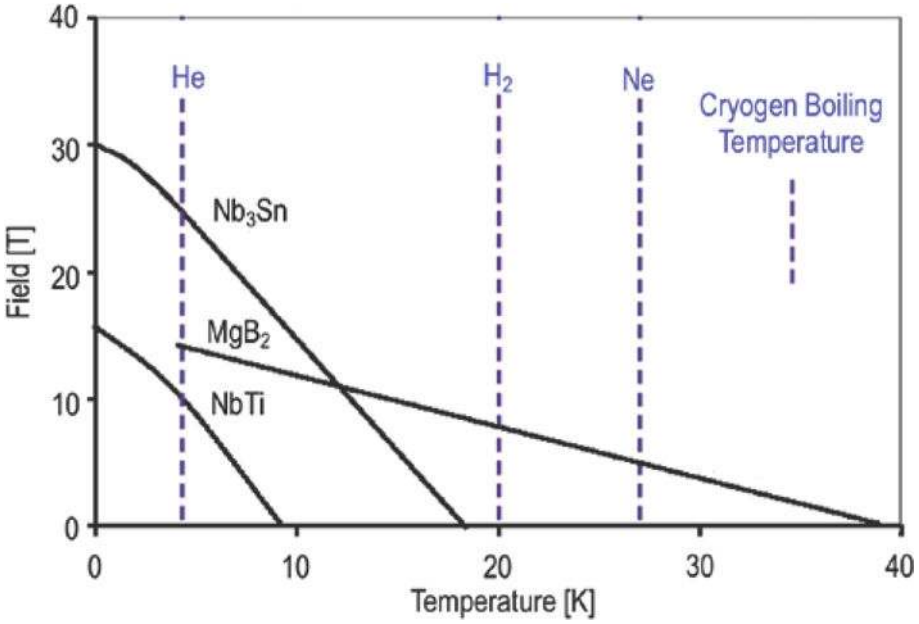

Fig. 5.

Field vs. temperature plots of MgB_2 and two LTS, Nb_3Sn, and NbTi, with three cryogens (He, H_2, Ne) and their atmospheric boiling temperatures, based on [23].

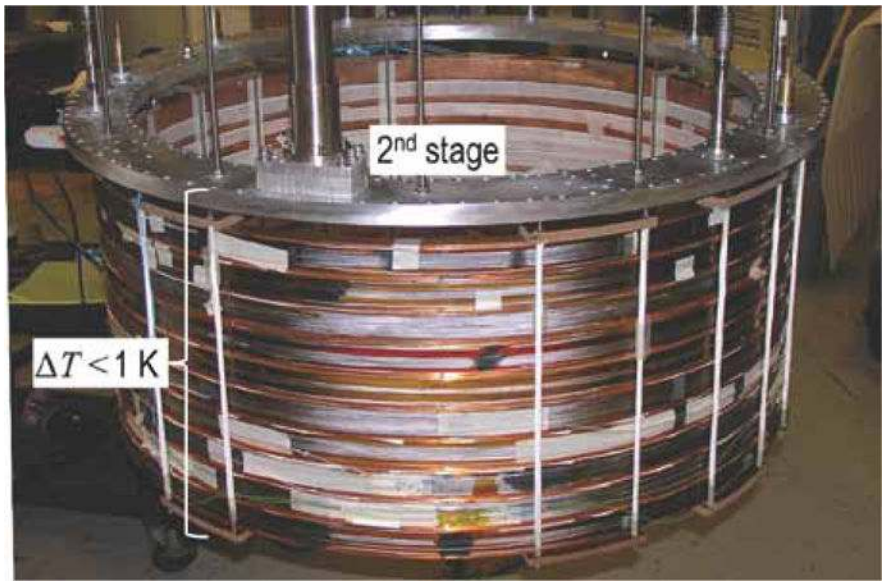

Fig. 6.
Photo of a 773-mm cold-bore 10-coil MgB_2 magnet with the SN2 can removed. Locations of the cryocooler 1st and 2nd stages are indicated.

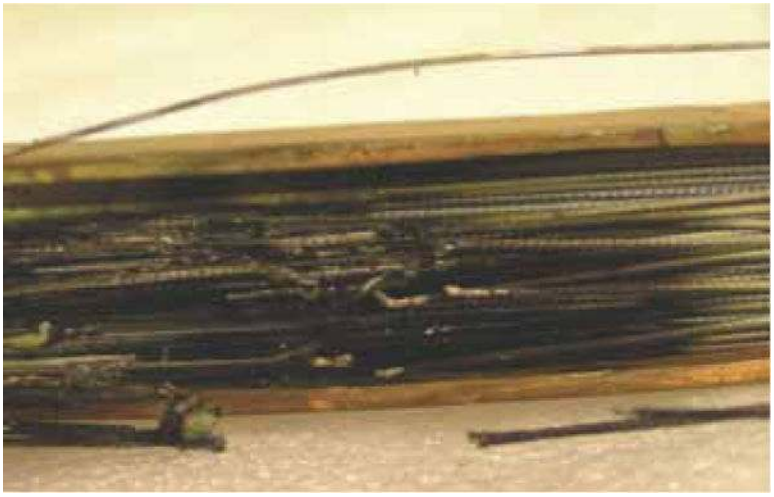

Fig. 7.
Photo of a damaged top coil winding section after a premature quench at 79 A.

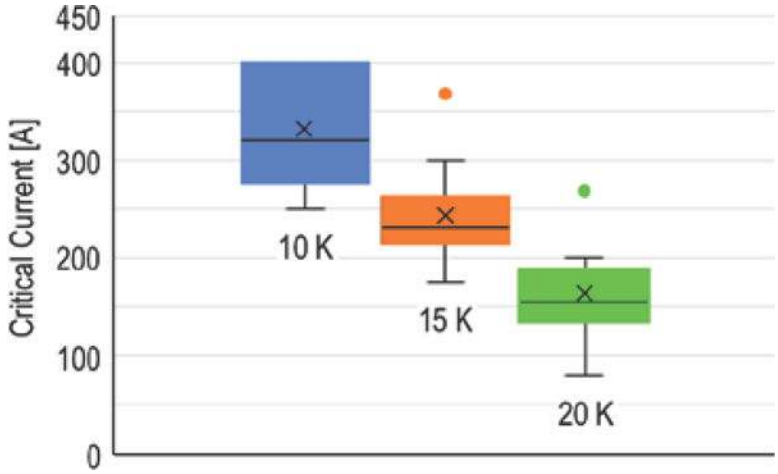

Fig. 8.
Critical current data of 10 joints in box-and-whisker plots.

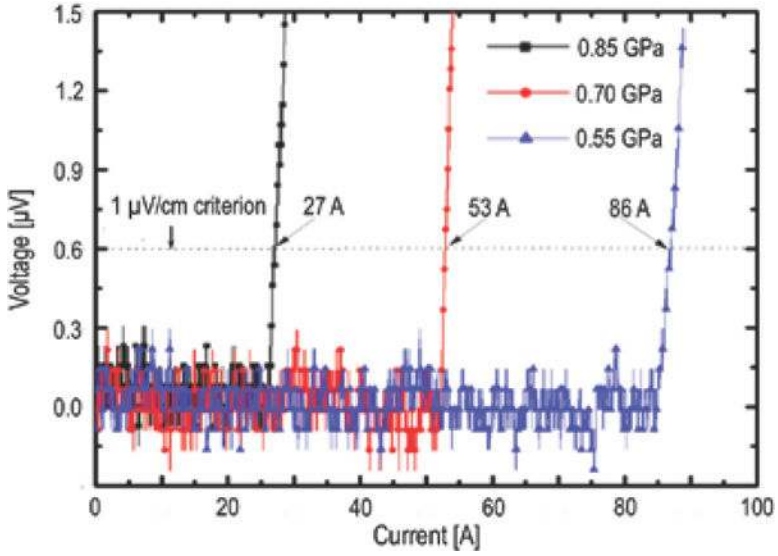

Fig. 9.

$V(I)$ plots at 10 K of *reacted* MgB_2 wire joints for three compressive pressures [30].

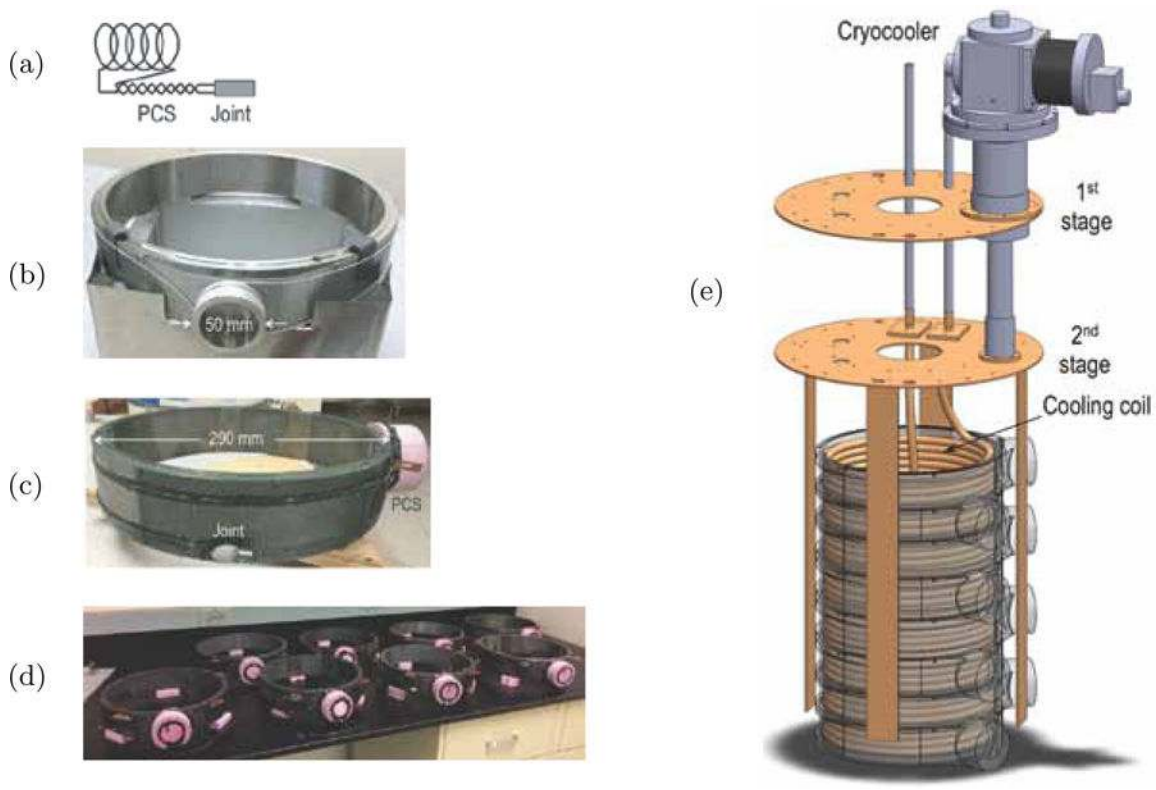

Fig. 10.

a) Circuit model of a coil-PCS-joint module; b) and c) photos of a module showing in foreground the PCS and the joint; d) photo of the 8 coil-PCS-joint modules; e) in-scale schematic drawing of the magnet assembly with a cryocooler and cooling coil [32].

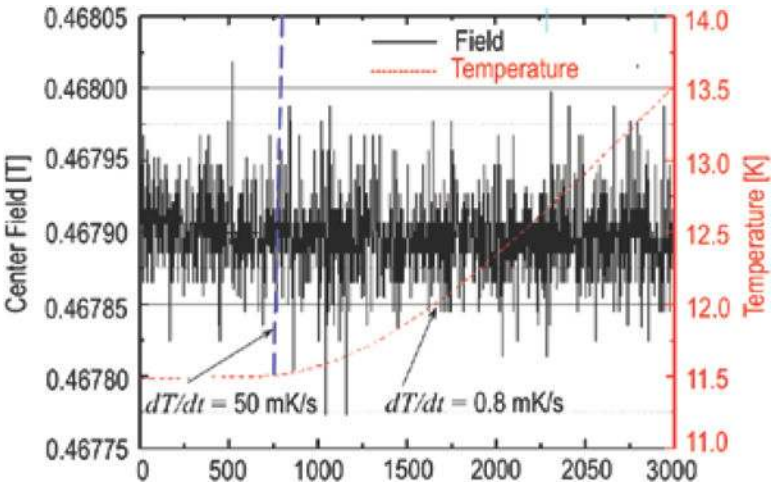

Fig. 11.
Center field and magnet temperature vs. time plots, based on [32].

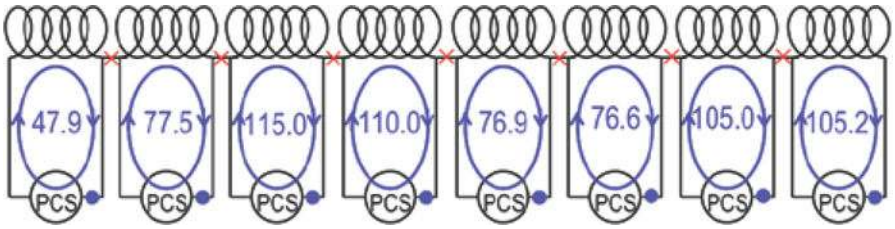

Fig. 12.

Computed, by the least square method, persistent-mode currents at 13 K among 8 coil-PCS-joint modules (center field: 0.47 T) after the magnet had warmed up from 9 K when it was put into persistent-mode operation at 100 A [32]. Blues dots and red crosses are joints, respectively, superconducting and resistive.

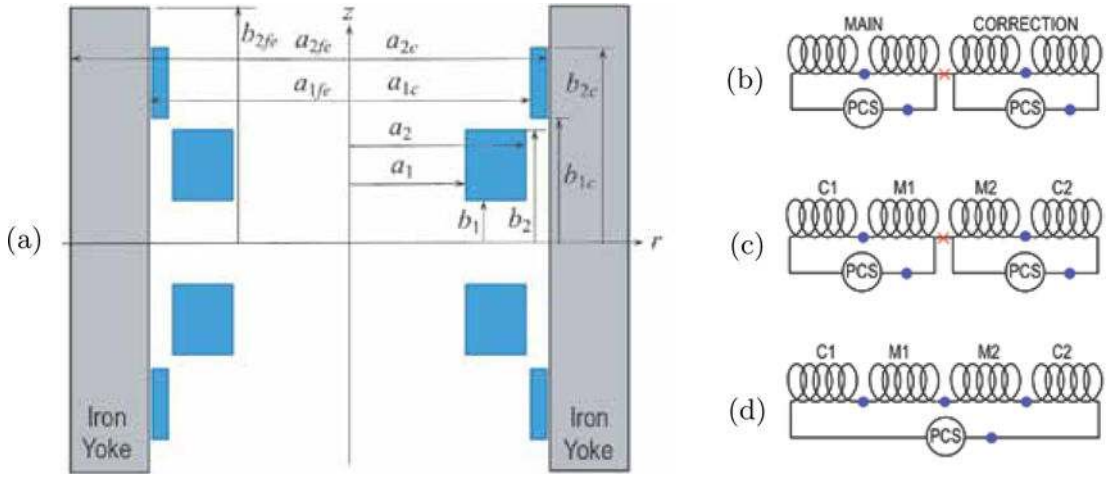

Fig. 13.

MgB_2 "finger" MRI magnet [34]. (a) Cross section: Main coils (large blue blocks)—M1 (top) and M2 (bottom); Correction coils (small blue rectangles); iron yoke. Circuit models: (b) two 2coils-PCS-2joints modules; (c) same as (b) except top and bottom modules respectively; (d) one 4coils-PCS-4joints module. Joints: blue dots (superconducting); red cross (resistive).

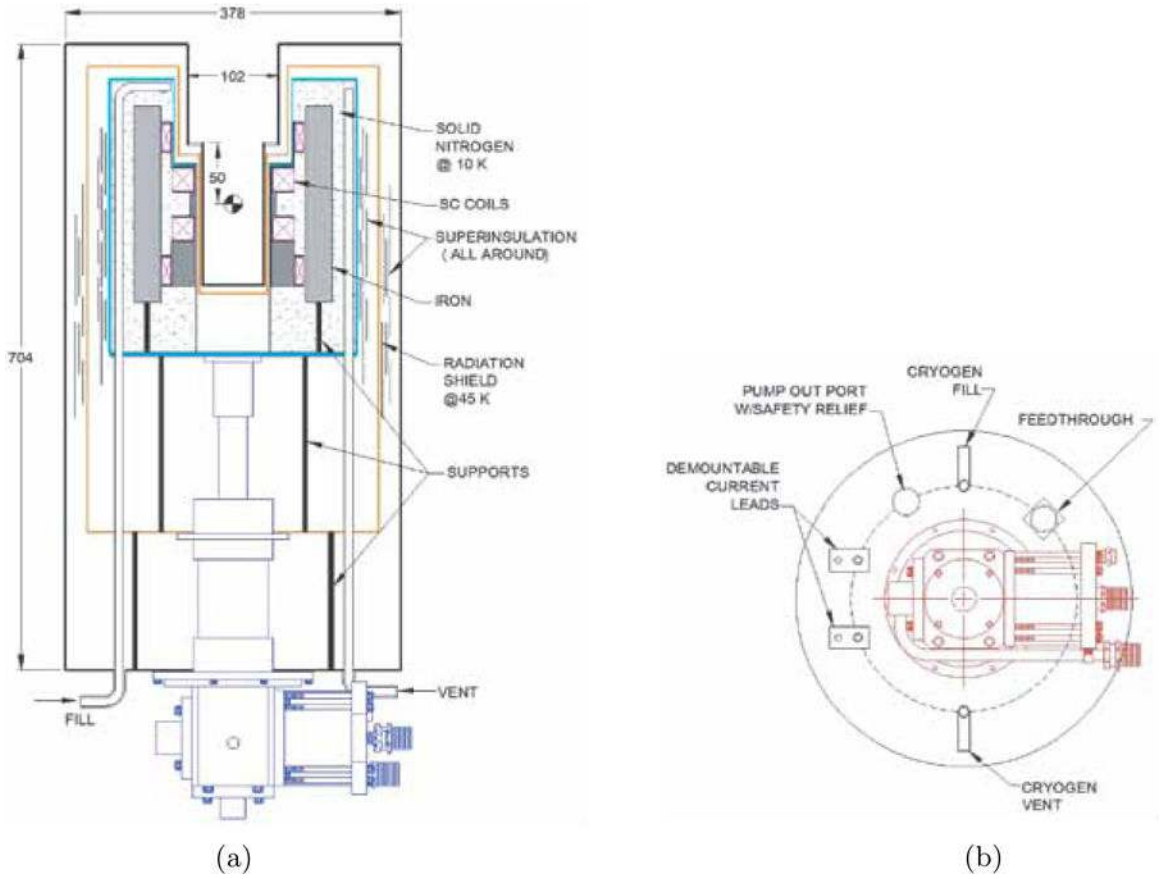

Fig. 14.
Overall setup views (a) side; (b) bottom [34]. Dimensions are in mm.

Table 1

Selected Values of T_{op}, ΔT_{op}, and Δe_h

T_{op} [K]	ΔT_{op} [K]	Δe_h [kJ/m^3]	Magnets
2.3	0.25	0.1	12-T NbTi
4.2	0.5	0.5	8-T NbTi
4.2	1	1	5-T NbTi
4.2	5	15	REBCO
10	5	80	MgB_2
30	10	4,000	REBCO
60	10	15,000	REBCO

Table 2

Magnet Parameters [4, 5]

Parameters	
Winding i.d.; o.d.; overall length [mm]	75; 107; 47.1
# of turns/DP coil	140
Bi2223 I_c at 77 K, self field [A]	140
Bare conductor width [mm]	3.2
Bare conductor thickness [mm]	0.23
Conductor length/DP coil [m]	42
# of DP coils; total # of turns	6; 840
Self inductance [mH]	50.4
Approximate I_{op} at 40 K [A]	20
Nominal operating temperature range [K]	20–40
Center field at I_{op} [T]	0.21
Maximum axial field [T]	0.29
Maximum radial field [T]	0.17

Table 3

Coil Parameters

Parameters	
Winding i.d.; o.d.; length [mm]	770; 798; 25.4
# turns/layer	25
# layer	16
Bare wire diameter [mm]	0.83
Insulated wire diameter [mm]	1.01
Single coil center field at 100 A [T]	0.06
Single coil peak field at 100 A [T]	0.71
Magnet center field at 100 A [T]	0.5
Magnet peak field at 100 A [T]	1.2
Operating temperature range at 100 A [K]	10–15

Table 4

Thermal Conductivity k [3]

	LHe		SN2			Epoxy		
Temperature [K]	**4.2**	**5**	**10**	**20**	**5**	**10**	**20**
k [mW/cm K]	0.2	40	15	4	0.4	1	2.5

Table 5

MgB_2 "Finger" MRI Magnet Parameters [34]

Parameters	
Main (2×Coil) Total wire length [m] a_1; a_2; b_1; b_2 (see Fig. 13) [mm] # Layers; Total turns	2 × 241 45.0; 68.5; 15.2; 40.2 27; 675
Correction (2×Coil) Total wire length [m] a_1; a_2; b_1; b_2 (see Fig. 13) [mm] # Layers; Total turns	2 × 155 70.0; 79.7; 60.0; 90.0 11; 330
Iron Yoke (Top half) Total mass [kg] a_{1fe}; a_{2fe}; b_{2fe} [mm]	35 70.7; 107.7; 110.0
Operating temperatures, nominal/peak [K]	14; 17
With iron yoke I_{op} (both coils) [A] λJ @ I_{op} [A/mm^2] Magnetic energy @ I_{op} [kJ]	107.9 124 1.6
Magnet fields, center/peak @ I_{op} [T] I_c @2 T & 17 K [A] Raw error field, 20-mm DSV [ppm]	1.5/2.0 145 260
SN2 mass [kg] Enthalpy [kJ]/Time [hr], 14→17 K	9.5 (≃ 9.2) liters 10.5/~10